Acta Biomaterialia 55 (2017) 410–419

Contents lists available at ScienceDirect

Acta Biomaterialia

journal homepage: www.elsevier.com/locate/actabiomat

Full length article

Non-invasive tracking of hydrogel degradation using upconversion nanoparticles

Yuqing Dong [a,b,c,1], Guorui Jin [b,c,1], Changchun Ji [b,c], Rongyan He [b,c], Min Lin [b,c], Xin Zhao [e], Ang Li [d], Tian Jian Lu [b,c,*], Feng Xu [b,c,*]

[a] State Key Laboratory for Mechanical Behavior of Materials, School of Materials Science and Engineering, Xi'an Jiaotong University, Xi'an 710049, PR China
[b] The Key Laboratory of Biomedical Information Engineering of Ministry of Education, School of Life Science and Technology, Xi'an Jiaotong University, Xi'an 710049, PR China
[c] Bioinspired Engineering and Biomechanics Center (BEBC), Xi'an Jiaotong University, Xi'an 710049, PR China
[d] Key Laboratory of Shaanxi Province for Craniofacial Precision Medicine Research, College of Stomatology, Xi'an Jiaotong University, Xi'an 710049, PR China
[e] The Interdisciplinary Division of Biomedical Engineering, The Hong Kong Polytechnic University, Hung Hom, Hong Kong Special Administrative Region

ARTICLE INFO

Article history:
Received 13 December 2016
Received in revised form 13 April 2017
Accepted 13 April 2017
Available online 17 April 2017

Keywords:
Hydrogels
Degradation
Upconversion nanoparticles
Non-invasive tracking

ABSTRACT

Tracking the distribution and degradation of hydrogels *in vivo* is important for various applications including tissue engineering and drug delivery. Among various imaging modalities, fluorescence imaging has attracted intensive attention due to their high sensitivity, low cost and easy operation. Particularly, upconversion nanoparticles (UCNPs) that emit visible lights upon near-infrared (NIR) light excitation as tracking probes are promising in deciphering the fate of hydrogels after transplantation. Herein, we reported a facile and non-invasive *in vivo* hydrogel tracking method using UCNPs, where the degradation of hydrogels was determined using the decrease in fluorescence intensity from the UCNPs encapsulated in the hydrogels. We found that the change in the fluorescence intensity from the UCNPs was well consistent with that of the fluorescein isothiocyanate (FITC) covalently conjugated to hydrogels and also with the weight change of the hydrogels, suggesting the accuracy of the UCNPs in tracking the degradation of hydrogels. Furthermore, the *in vivo* fluorescence signals were only observed from the UCNPs instead of FITC after implantation for 7 days due to the deep tissue penetration of UCNPs, demonstrating the capability of UCNPs in longitudinal, consecutive and non-invasive monitoring the *in vivo* degradation of hydrogels without causing any damage to the major organs (heart, lung, liver and kidney) of model rats. This study thus paves the way for monitoring the *in vivo* behaviors of biomimetic materials via deep tissue imaging with great clinical translation potentials.

Statement of Significance

Long-term noninvasive *in vivo* tracking of the distribution and degradation of biodegradable hydrogels using fluorescent probes is important in tissue regeneration and drug delivery. Unlike the widely used fluorescent dyes and quantum dots (QDs) that suffer from photobleaching and undesired toxicity, upconversion nanoparticles (UCNPs) with high stability, deep tissue penetration as tracking probes are promising in deciphering the fate of hydrogels after transplantation. Herein, we reported a noninvasive *in vivo* hydrogel tracking method using UCNPs and found that the fluorescence intensity change from the UCNPs was well consistent with the weight change of the hydrogels, suggesting the accuracy of UCNPs in tracking hydrogel degradation. This study provides inspirations on developing advanced NIR light regulated probes with great clinical translation potentials.

1. Introduction

Biodegradable hydrogels are water-swollen polymer networks with widespread applications in tissue regeneration, drug delivery and surgical implants due to their tunable biophysical and biochemical properties [1,2]. Appropriate degradation of hydrogel is

* Corresponding authors at: The Key Laboratory of Biomedical Information Engineering of Ministry of Education, School of Life Science and Technology, Xi'an Jiaotong University, Xi'an 710049, PR China.
E-mail addresses: tjlu@mail.xjtu.edu.cn (T.J. Lu), fengxu@mail.xjtu.edu.cn (F. Xu).
[1] Authors contributed equally.

http://dx.doi.org/10.1016/j.actbio.2017.04.016
1742-7061/

required to match the pace of neo-tissue formation, which ensures the structural and functional integration of implanted hydrogels with the host tissue for progressed tissue regeneration [3–6]. Quick degradation may lead to insufficient support for tissue ingrowth, whereas slow degradation may hinder the neo-tissue formation and result in fibrosis [7]. Also, degradation of hydrogel is highly relevant to the release mechanism of the drugs encapsulated in the hydrogels, which is important for the design and development of formulations with controlled release kinetics [8]. Therefore, it is extremely crucial to track the *in vivo* degradation of hydrogel to match the material degradation with tissue regeneration and/or to tune the drug release kinetics.

Efforts have been devoted for monitoring of hydrogels degradation by measuring the changes of hydrogels in terms of mechanical properties, molecular weight, matrix weight, morphology and viscosity [9,10]. However, these methods are invasive and inconsecutive in monitoring the dynamic behaviors of implanted hydrogels. For instance, the *ex vivo* histological staining is a common method for determining the resorption of biomaterials, which needs to sacrifice significant amount of animals limiting its clinical applications. Therefore, monitoring the degradation of hydrogels in a real-time and non-invasive manner has attracted increasing attentions. With the help of molecular imaging modalities such as magnetic resonance imaging (MRI) [11], positron emission tomography (PET) [12] and fluorescence imaging [13], people can visualize the degradation of biomaterials and their interactions with surrounding tissues in living systems in real-time and non-invasive ways [14,15]. Among these imaging modalities, fluorescence imaging offers advantages in providing a maneuverable nonionizing platform to track the *in vivo* fate of biomaterials, drugs and cells due to its easy setup, low cost, high sensitivity, non-invasiveness and long-term observation [16–18]. For instance, fluorescent dyes (*e.g.*, fluorescein-5-carboxyamido hexanoic acid, Alexa Fluor 647 and protoporphyrin) have been covalently attached to hydrogels for monitoring the degradation of hydrogels *in vivo* based on the decay in fluorescence signals [19–21]. Quantum dots have been entrapped within collagen and silk hydrogels for tracking hydrogel degradation based on the reduction of fluorescence intensity of hydrogels [22,23]. However, these fluorescent probes usually suffer from poor stability, biocompatibility and biodegradability, which may hinder their applications for *in vivo* hydrogel tracking [24,25]. Moreover, decorating the fluorescent dye onto the hydrogel is a complex route, and fluorescent labels may affect the degradation pattern [26]. Besides, fluorescent dyes and quantum dots require excitation of UV or visible lights, which have limited penetration depth into biological tissues because they can be largely absorbed by the skin and underlying fat tissues [27], limiting their *in vivo* applications.

Upconversion nanoparticles (UCNPs) that emit visible lights upon near-infrared (NIR) light excitation hold great promise to address the above mentioned issues [28], due to their advantages of large anti-Stokes shifts, long lifetimes, high photostability, reduced auto-fluorescence, no blinking, and deep tissue penetration [29–31]. Because of these merits, UCNPs have been intensively applied in bioimaging and cell tracking [32,33]. Non-invasive monitoring of hydrogel degradation using UCNPs has also been explored [34]. However, the *ex vivo* tracking hydrogels embedded within the cultured intervertebral discs using UCNPs cannot precisely predict their *in vivo* behaviors such as degradation, retention and engraftment, due to the complicated and dynamic *in vivo* microenvironment. In addition, the hydrogel degradation results obtained by using UCNPs as the only tracking probe are not convincing because of the potential leakage of the physically mixed UCNPs from hydrogels. Therefore, the capability of UCNPs in tracking the degradation of hydrogels in living animals needs to be evaluated urgently, using a chemically conjugated fluorescent reporter as the benchmark to confirm the reliability of UCNP in *in vivo* hydrogel tracking.

In this contribution, we used $NaYF_4$:Yb,Er@PAA UCNPs as NIR regulated fluorescent probe for non-invasive tracking of hydrogel degradation both *in vitro* and *in vivo* in a rat model (Scheme 1) with fluorescein isothiocyanate (FITC) that can be covalently modified onto hydrogel polymer chains as the benchmark. The model hydrogels were gelatin methacryloyl (GelMA) hydrogels that are widely applied in various biomedical applications [35–39]. To this end, $NaYF_4$:Yb,Er@PAA UCNPs were physically mixed within FITC-modified GelMA hydrogels and the fluorescence intensity changes from UCNPs and FITC are well consistent with the weight changes of GelMA hydrogels, confirming the capability of UCNPs in precise tracking of hydrogel degradation. Then the capability of UCNPs in long-term tracking of the degradation of GelMA hydrogel was evaluated *in vivo* by embedding the UCNP-labeled GelMA hydrogels into rat abdomens. The gradual decrease in fluorescence signals from UCNPs in the transplanted site can be monitored for 7 days, suggesting the degradation of GelMA hydrogels *in vivo*. However, no fluorescence signals were observed from FITC due to the limited tissue penetration of its excitation light. The fluorescence signal changes of UCNPs and FITC obtained from tissue section slides under confocal microscope are in similar trends, confirming the accuracy of *in vivo* hydrogel tracking with UCNPs. The safety of UNCPs in long-term hydrogel tracking was proved by the histological staining of the tissue sections from different organs compared with the ones without hydrogel implantations. These results confirm the capability of UCNPs in longitudinal and consecutive monitoring the degradation of hydrogels *in vivo*.

2. Materials and methods

2.1. Synthesis and characterization of $NaYF_4$:Yb,Er@PAA UCNPs

The synthesis of UCNPs was carried out by a thermal decomposition procedure. In a typical synthesis of 30 nm sized β-$NaYF_4$:Er/Yb, $YCl_3{\cdot}6H_2O$ (242.69 mg, 0.8 mmol), $YbCl_3{\cdot}6H_2O$ (69.75 mg, 0.18 mmol), and $ErCl_3{\cdot}6H_2O$ (7.64 mg, 0.02 mmol) were dissolved in 2 mL ultrapure water and then added into a flask containing 15 mL 1-octadecene and 7.5 mL oleic acid. The obtained solution was stirred at room temperature for 0.5 h. Afterwards, the mixture was slowly heated to 120 °C and then kept for 1 h at 156 °C to remove ultrapure water under argon atmosphere protection and then cooled down to room temperature. Next, 10 mL methanol solution of NH_4F (148.15 mg, 4 mmol) and NaOH (100 mg, 2.5 mmol) were added into the solution and kept stirring at room temperature for 2 h. After methanol evaporation, the solution was heated to 280 °C and maintained for 1.5 h, then cooled down to room temperature. The resulting product was centrifuged and washed with ethanol and cyclohexane for three times and was finally re-dispersed in 10 mL cyclohexane. To modify the surface of UCNPs, a ligand exchange process was performed using poly (allylamine hydrochloride) (PAA) as a multidentate ligand that displaces the original hydrophobic ligands on the surface of UCNPs by mixing 1 mL ethanol, 1 mL of UCNPs and 14.5 μL PAA, dispersed in chloroform (~15 mg/mL) with overnight stirring. The solution was then centrifuged at 10,000 rpm for 12 min. After being washed three times with ethanol and ultrapure water, the particles were re-dispersed in 5 mL ultrapure water.

The morphologies of the samples were obtained by transmission electron microscopy (TEM) using a JEM 2100 instrument at an accelerating voltage of 200 kV. The as-prepared samples were characterized by powder X-ray diffraction (XRD) on an XRD-7000 diffractometer with Cu Kα radiation. The FTIR spectra of the nanoparticles were obtained using a Nicolet iS50 Fourier transform

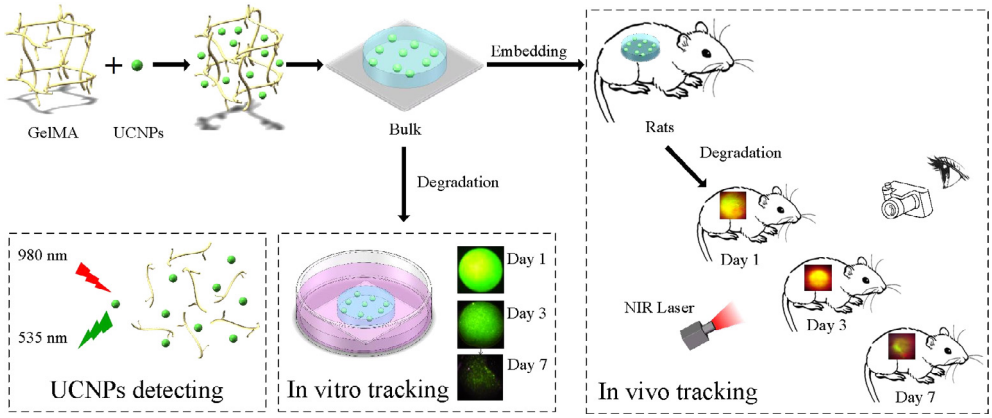

Scheme 1. Schematic illustration of the synthesis of GelMA hydrogel physically mixed with $NaYF_4$:Yb,Er@PAA UCNPs and followed by *in vitro* and *in vivo* tracking the degradation of hydrogels using upconversion nanoparticles.

infrared spectrophotometer (Thermo Electron Co., USA) by the KBr method. The upconversion emission spectra were recorded by using a spectrophotometer (QuantaMasterTM40) under external excitation of a 250 mW 980 nm laser diode (RGB Lasersystems). Images of printed patterns upon excitation using a 980 nm CW laser and 360 nm UV laser (Changchun Liangli Photoelectric Co., Ltd) were obtained via a Nikon D90 digital Single Lens Reflex with Macro lens with a 500–700 nm bandpass filter. All the measurements were performed at room temperature.

2.2. Cytotoxicity study of $NaYF_4$:Yb,Er@PAA UCNPs

The metabolic activity of NIH-3T3 cells was evaluated by met hylthiazolyl-diphenyl-tetrazolium bromide (MTT) assays to study the cytotoxicity of UCNPs. NIH-3T3 cells were seeded in 96-well plates (Costar, IL, USA) at 1×10^4 cells/mL. After 24 h incubation, the medium was replaced by 100 μL of the UCNPs suspension at concentrations of 20, 40 and 60 mg/mL, and the cells were then incubated for 48 and 72 h, respectively. After the designated time intervals, the wells were washed twice with 1 × PBS buffer and 100 μL of freshly prepared MTT (0.5 mg/mL) solution in culture medium was added into each well. The MTT medium solution was carefully removed after 3 h incubation in the incubator at 37 °C. DMSO (100 μL) was then added into each well and the plate was gently shaken to dissolve all the precipitates formed. The absorbance of MTT at 570 nm was monitored by using the microplate reader (Genios Tecan). Cell viability was expressed by the ratio of absorbance of the cells incubated with UCNP suspension to that of the cells incubated with culture medium only.

$$\text{Cell viability } (100\%) = \frac{\text{Absorbance of UCNP} - \text{treated Cells}}{\text{Absorbance of UCNP free Cells}} \times 100\%$$

2.3. Synthesis of GelMA

Synthesis of GelMA was described previously [38]. Briefly, 20 g of gelatin from porcine skin (Sigma-Aldrich, China) was dissolved in 200 mL of phosphate buffered saline (PBS, 1X, Invitrogen) at 50 °C using magnetic stirrer. Then, 16 mL methacrylic anhydride (Sigma-Aldrich, China) was added to react with the gelatin solution under vigorous stirring for 3 h at 60 °C. After that, the solution was transferred into a dialysis membrane with 12–14 kDa cut-off in distilled water at 40 °C for removing the salts and other small molecules. The distilled water was changes 2 to 3 times every day. After dialysis for 7 days, the GelMA solution was filtered with a sterile filter and transferred to 50 mL-Falcons. The solution was then freeze-dried to obtain GelMA foam that was stored at −80 °C before use.

2.4. Conjugation of FITC onto GelMA hydrogel network

To conjugate FITC onto GelMA hydrogel network, 1 g freeze-dried of GelMA was dissolved in 50 mL of sodium bicarbonate (Sigma-Aldrich) aqueous solution (100 mM) at 40 °C, and 20 mg of FITC was dissolved in 10 mL dimethyl formamide (DMF, EMD chemicals). The two solutions were mixed and reacted for 6 h at 40 °C. The resultant solution was dialyzed against distilled water at 40 °C for 7 days, and lyophilized to obtain solid FITC-GelMA. The reaction and purification were performed in the dark to minimize fluorescein photobleaching.

2.5. Fabrication of UCNP-labeled GelMA hydrogel

To fabricate GelMA hydrogel incorporated with $NaYF_4$:Yb, Er@PAA UCNPs, 1 g freeze-dried of GelMA foam was dissolved in 2 mL of distilled water and then 10 μL crosslinking agent (2-Hydr oxy-2-methylpropiophenone) was added into GelMA solution with slight shacking. The prepolymer solution was further mixed with 400 μL $NaYF_4$:Yb,Er@PAA UCNPs solution (40 mg/ml). Then, the mixed solution was pipetted into a mold (high 3 mm; diameter 11 mm) as shown in Fig. S1 and exposed to 6.9 mW cm^{-2} UV light (365 nm) for a certain period of time to yield UCNP labeled-GelMA hydrogels with white color. The protocol of synthesizing UCNP and FITC dual labeled-GelMA hydrogels with yellow green color was similar with the description above.

2.6. Tissue penetration evaluation of UCNPs for in vitro hydrogel tracking

One clean cuvette was injected with 1 mL of transparent UCNP-labeled GelMA solution (40 mg/mL) and the other cuvette was injected with 1 mL of green FITC-labeled GelMA solution. Then fresh slices of chicken breast meat (SCBM) with different thickness (2 mm, 6 mm and 10 mm) were covered on the top of the cuvettes, respectively. The NIR (980 nm) and UV (365 nm) lasers with the same output power (50 mW cm^{-2}) were located perpendicularly to the tissue slices covered on the top of the cuvettes, respectively. The fluorescence images from both UCNPs and FITC were captured in darkroom using a Nikon D90 digital Single Lens Reflex with Macro lens attached with UV filter (wavelength pass <700 nm) or IR filter (wavelength pass >500 nm), respectively. In addition, the

parameters of the camera such as exposure time (4 s) and aperture (F3.3) remain unchanged through experiments.

2.7. In vitro tracking of GelMA degradation using UCNPs

The UCNP and FITC dual labeled 10% crosslinked UCNP-FITC-GelMA hydrogels were located into culture dish and then immersed in 3 mL 1 × PBS solution, which was refreshed every day. The *in vitro* tracking of GelMA degradation using UCNPs was carried out for 7 days. After every 24 h, the hydrogels were put on a coverslip to take fluorescence images in the darkroom and the parallel control samples were measured to obtain the dry weight of hydrogels. Then software ImageJ (NIH, USA) was used to calculate the mean fluorescence intensity of hydrogels that is reflected by the mean gray value of the fluorescence region after subtracting the background fluorescence from the fluorescence images captured at designed time intervals. We notice that the change in mean gray value may not reflect the weight change if the hydrogels are in different physical properties (such as shape, volume et al.). To avoid the potential error caused by the difference in hydrogel physical properties, we used a mold as shown in Fig. S1 to fabricate hydrogels and the same dosage of hydrogel solution is used and strictly controlled. In this contribution, the volume and shape of the hydrogels are nearly the same in this study. Therefore, the change of hydrogel mean gray value can reflect the hydrogel weight change in this study. For further evaluation of the capability of $NaYF_4$:Yb,Er@PAA UCNPs in accurate tracking of hydrogel degradation with different crosslink intensity and liquid environment, we put 5% and 10% UCNPs-GelMA hydrogels into 3 mL mixture of 1 × PBS solution supplemented with 0.25% trypsin and 2.21 mM EDTA solution and 3 mL 1 × PBS solution respectively. The fluorescent images of the UCNP-labeled hydrogels were taken every hour, meanwhile the dry weight of the control samples were measured.

2.8. In vivo tracking of GelMA degradation using UCNPs

All animal studies were performed in compliance with the guidelines in the Declaration of Helsinki and the project protocols were approved by the Animal Ethics Committee of Xi'an Jiaotong University. The Sprague–Dawley rats were purchased and fed in the animal center at the medical school of Xi'an Jiaotong University. Healthy rats with body weight around 400 g were selected for *in vivo* hydrogel tracking study. The synthesized 5% UCNP-FITC-GelMA hydrogels bulks were first embedded into rat abdomen, which is nearly 6 mm under the skin. We marked the hydrogels location and took fluorescent images on day 1, 3, 5 and 7 when the rats were anesthetized with 1–2% isoflurane. Meanwhile, the rats in the parallel control group were euthanized at the designed time intervals and the remained hydrogels were collected for dry weight measurement. The *in vivo* tracking of GelMA degradation using UCNPs has been prolonged for 15 days. The fluorescent images of hydrogels that were embedded into rat abdomen were captured on day 3, 5, 10 and 15. Meanwhile, we perpendicularly inserted hydrogels into rat leg muscular tissue, which is nearly 10 mm under the skin. After 7 days, we obtained tissues from the hydrogel-implanted sites and prepared tissue freezing microtome slices in 20 μm thickness and characterized the fluorescence changes by confocal microscopy.

2.9. Haematoxylin and eosin (H&E) staining

The histopathological analysis of rat organs such as heart, liver, lung and kidney were performed by H&E staining. These organs were obtained from the rats with UCNP-FITC-GelMA hydrogel implantation for 7 days and the control group was from the rats without hydrogel implantation. The tissues were collected and quickly fixed with 10% formalin overnight, followed by preservation with 70% ethanol to dehydrate, and then paraffin-embedded. Paraffin embedded tissues were cut (5 mm) and stained with H&E.

2.10. Western blot

To study the *in vivo* safety of UCNPs, western blot was performed by the chemiluminescence method as described previously [40]. The organs including lung, liver, spleen, kidney and heart were obtained from the rats with UCNP-FITC-GelMA hydrogel implantation and then electrophoresed, transferred to nitrocellulose. Briefly, aliquots of whole-tissue lysates containing 10 μg of total protein were separated on sodium dodecyl sulfate (SDS) gels and blotted onto nitrocellulose. The completeness of protein transfer was checked by Coomassie staining of the gel after blotting. After fixation with 0.5% glutaraldehyde, the blots were stained with Poceau S to test the quality of the protein transfer [41]. The fixation enables reuse of the same blot several times, thus saving labor and increasing the comparability of the blots generated with various antibodies. The blot was treated with the primary antibody, β-actin and caspase12 (Cell Signaling Technology) that was dissolved in tris-buffered saline containing 2% skim milk and 0.1% Tween, respectively and the treated blot was left overnight at 4 °C. After washing the blot, it was incubated with anti-rat IgG (Cell Signaling Technology) in tris-buffered saline containing 4% skim milk and 0.1% Tween for 2 h at room temperature. Primary antibody binding was visualized using secondary antibodies and an enhanced chemiluminescence (ECL) detection system. Then, the final samples were scanned using an Image Quant LAS 4000 instrument (GE Healthcare).

2.11. Statistical analysis

All quantitative results were obtained from at least three samples for analysis. Data were expressed as the mean ± standard error of the mean. A two-tailed paired Student's *t*-test was used to compare the differences. Difference with $p < 0.05$ was considered to be statistically significant.

3. Results and discussion

3.1. Characterization of $NaYF_4$:Yb,Er@PAA UCNPs

The fluorescence spectrum of $NaYF_4$:Yb,Er@PAA UCNPs was shown in Fig. 1A, which demonstrated the upconversion fluorescent peaks centered at 535 nm and 655 nm, respectively. The morphology and size of the $NaYF_4$:Yb,Er@PAA UCNPs were characterized by TEM. Uniformly distributed typical hexagonal morphology with a diameter around 35 nm (insert left) was observed. The bright fluorescence (insert right) was clearly observed from the fluorescent images of UCNPs that were captured in the dark field. To confirm the identity of the UCNPs, X-ray diffraction analysis was performed. As shown in Fig. 1B, the peak positions and intensities of the synthesized UCNPs agree well with the calculated line pattern for hexagonal-phase $NaYF_4$ (JCPDS card), indicating that these UCNPs have pure hexagonal morphology with high crystallinity [42,43]. To improve the biocompatibility and water dispensability of UCNPs, the synthesized $NaYF_4$:Yb,Er@OA UCNPs were further decorated with water-soluble polyacrylic acid (PAA) to obtain the NaYF4:Yb,Er@PAA UCNPs, and the successful decoration of PAA was verified by the Fourier transform infrared spectroscopy (FTIR) (Fig. 1C). The broad band of UCNPs@OA and UCNPs@PAA was at approximately 3445.3 and 3447.2 cm^{-1}, respectively, which were corresponding

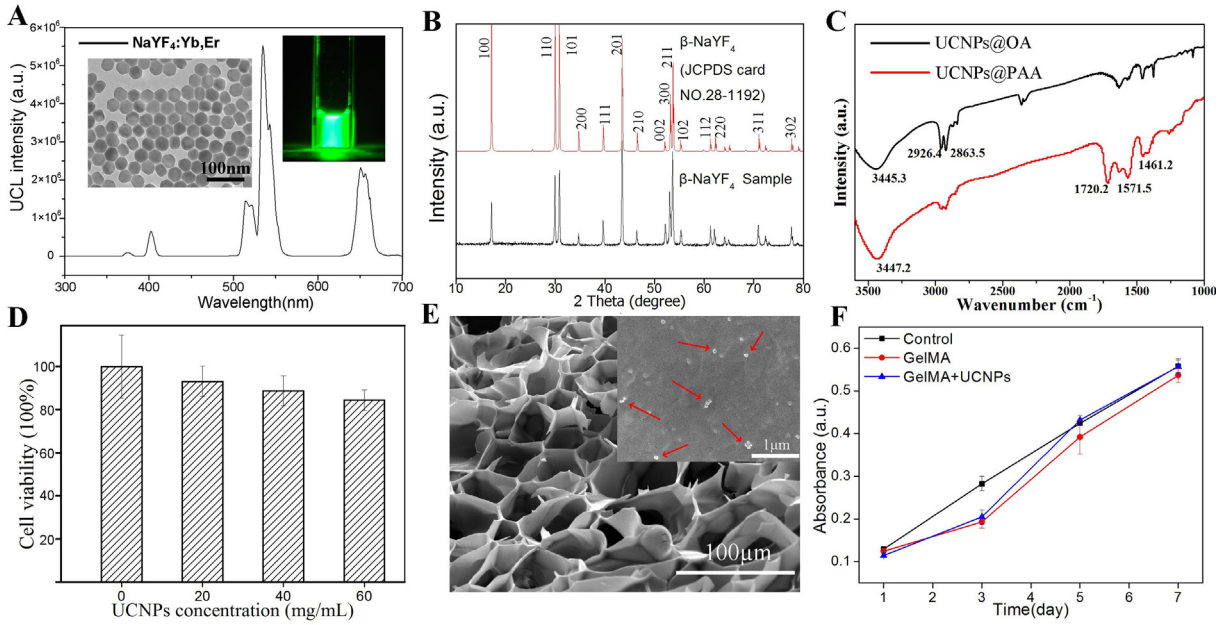

Fig. 1. Characterization of $NaYF_4$:Yb,Er@PAA UCNPs and cell proliferation on UCNP-labeled GelMA hydrogels. (A) Fluorescence spectrum of $NaYF_4$:Yb,Er@PAA UCNPs under the 980 nm excitation. The inserts show the TEM morphology of UCNPs and the fluorescent image of UCNPs in a cuvette, respectively. (B) XRD pattern of $NaYF_4$:Yb,Er@PAA UCNPs (black) and JCPDS card (red); (C) FITR spectra of $NaYF_4$:Yb,Er@PAA UCNPs (red) and UCNPs without coating (black). (D) The metabolic viabilities of NIH 3T3 cells after incubation with 20, 40 and 60 mg/mL $NaYF_4$:Yb,Er@PAA UCNPs for 48 h, respectively. (E) SEM image of $NaYF_4$:Yb,Er@PAA UCNP-labeled GelMA hydrogel. The insert shows the UCNPs (indicated by the red arrow) within hydrogel under high magnification. (F) The proliferation profiles of NIH 3T3 cells incubated with 40 mg/mL $NaYF_4$:Yb,Er@PAA UCNP-labeled GelMA hydrogels for 7 days in culture medium using UCNP-free GelMA hydrogels as control. (For interpretation of the references to colour in this figure legend, the reader is referred to the web version of this article.)

to the O–H stretch vibration. The transmission bands of UCNPs@OA at 2926.4 and 2863.5 cm^{-1} are assigned to the stretching vibration of methylene (CH_2) in the oleic acid molecules [44]. After the surface modification with PAA, the disappearance of the vibration at 2926.4 and 2863.5 cm^{-1} suggests the successful coating of PAA onto the particle surface [45]. Further, the two strong bands of UCNPs@PAA centered at 1571.5 and 1461.2 cm^{-1} were associated with the asymmetric and symmetric stretching vibrations of carboxylate anions on the surface of the UCNPs, respectively. Meanwhile, the strong band of UCNPs@PAA at 1720.2 cm^{-1} indicated the presence of the COOH groups on the particle surface, further confirming the successful coating of PAA on the surface of UCNPs [46].

The ideal fluorescent probes for hydrogel tracking should be non-toxic, photo-stable and with the capability of deep tissue penetration [24,29]. Therefore, the cytotoxicity of $NaYF_4$:Yb, Er@PAA UCNPs with four different concentrations of UCNPs (0 mg/mL, 20 mg/mL, 40 mg/mL and 60 mg/mL) was evaluated by co-culturing with NIH 3T3 cells for 48 h using MTT method, respectively (Fig. 1D). The viability of NIH 3T3 cells remained at above 84% after incubation with various concentrations of $NaYF_4$: Yb,Er@PAA UCNPs (20, 40 and 60 mg/mL). The $NaYF_4$:Yb,Er@PAA UCNP-treated NIH 3T3 cells and UCNP-free NIH 3T3 cells showed no significant difference ($p < 0.01$) in cell viability, suggesting the low cytotoxicity of $NaYF_4$:Yb,Er@PAA UCNPs to cells. The morphology of the synthesized GelMA hydrogel was characterized by SEM, from which we observed clear and typical porous network structure of hydrogel (Fig. 1E). Meanwhile, the effect of blending UCNPs within GelMA hydrogel on cell proliferation was also evaluated by MTT assay for 7 days (Fig. 1F). No significant difference was found in the cell proliferation between the UCNP-labeled and UCNP-free GelMA hydrogels, confirming the negligible effect of $NaYF_4$:Yb,Er@PAA UCNPs on the biocompatibility of GelMA hydrogels.

3.2. Tissue penetration evaluation of UCNPs for in vitro hydrogel tracking

In addition to low cytotoxicity, high photostability and deep tissue penetration of the fluorescent probes used in cell and biomaterial tracking are the two important criteria for achieving real-time and non-invasive hydrogel tracking for long duration. Quantum dots (QDs) as popular fluorescent probes have been incorporated in silk materials for studying silk biodegradation and distribution *in vivo*. However, the fluorescence of QD-incorporated silk microspheres was quenched within 24 h. Although the QD-incorporated silk hydrogels could attenuate the quenching of QDs, the labeled silk hydrogels could only be tracked around 4 days after subcutaneous injection into rats [23]. In addition, QDs suffer from potential degradation caused by reactive oxygen species [25], further resulting in fluorescence decrease and release of toxic heavy metal ions [47]. As compared to conventional down-conversion QDs and fluorescent dyes, UCNPs exhibit high photostability, because of their stable structure and the limited exposure to NIR light (980 nm) [22,48]. To evaluate the tissue penetration ability of $NaYF_4$:Yb,Er@PAA UCNPs, the fluorescent images of UCNP-labeled GelMA hydrogels in glass cuvette were obtained by letting the excitation light pass though slices of chicken breast meat (SCBM) with different thickness and a fluorescent dye FITC-labeled GelMA hydrogels were used as control group (Fig. 2).

We observed bright fluorescent emission from both UCNPs and FITC before covering SCBM under the excitation of NIR and UV light. However, the fluorescence intensity of FITC decreased significantly with increasing thickness of SCBM and no fluorescence signals could be observed when the thickness of the chicken chip reached 6 mm (Fig. 2). In contrast, strong fluorescent emission from UCNP-labeled GelMA hydrogels can still be observed even with the 6 or 10 mm thickness tissue coverage, demonstrating deep tissue penetration capability of UCNPs. This is because of

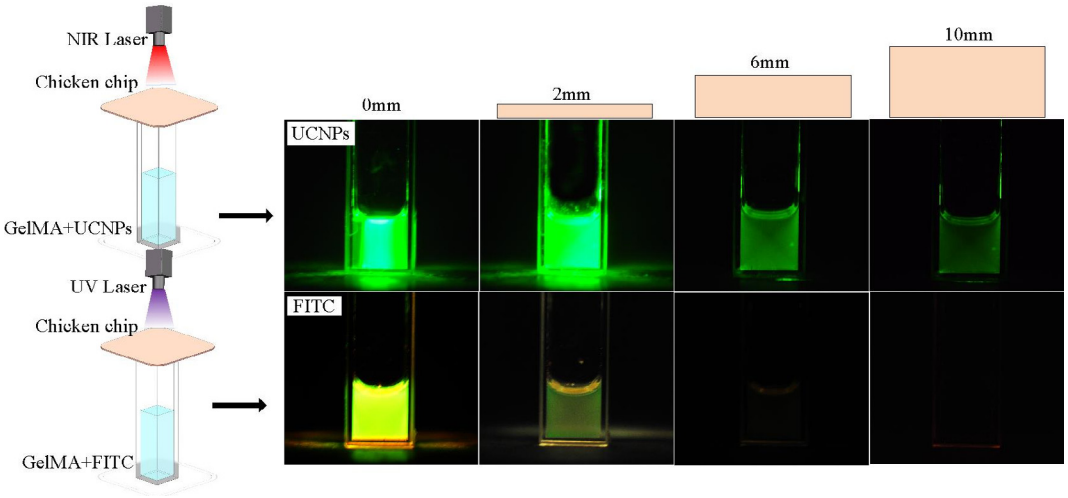

Fig. 2. Illustration of the experimental setup used to estimate the tissue penetration ability of UCNPs and FITC inside tissues. A slice of chicken breast meat with varying thickness (2 mm–10 mm) was placed between the laser source and the glass cuvette containing $NaYF_4$:Yb,Er@PAA UCNP-labeled hydrogel and FITC labeled hydrogel. NIR images showed upconversion emission from UCNPs.

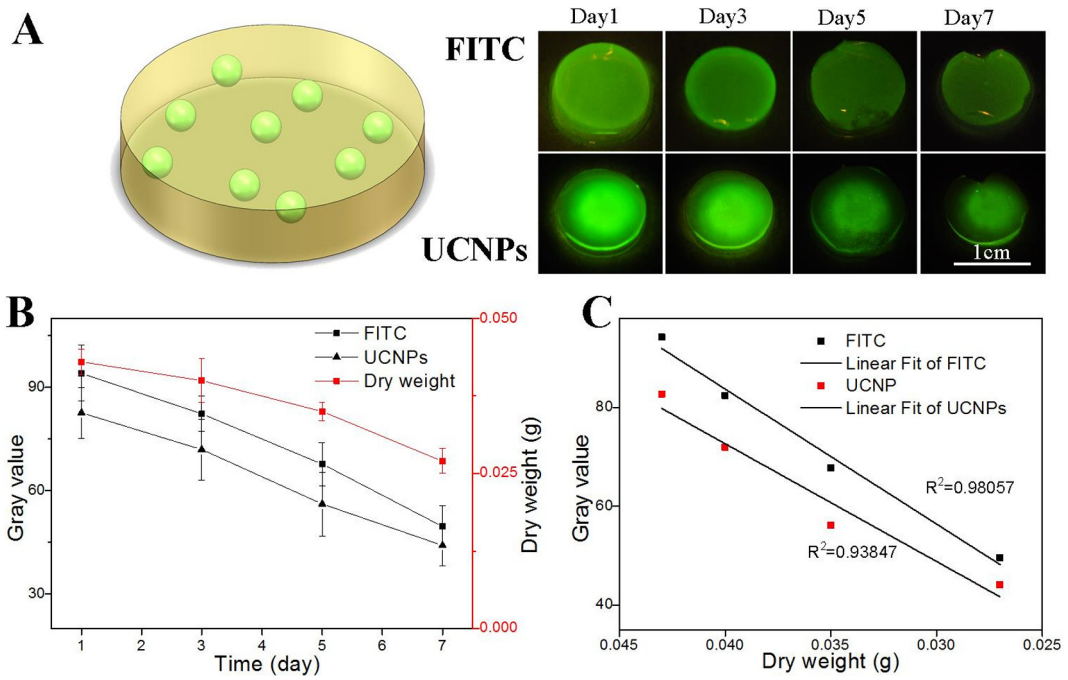

Fig. 3. *In vitro* tracking the degradation of hydrogels using $NaYF_4$:Yb,Er@PAA UCNPs. (A) Schematic illustration of UCNP and FITC dual labeled GelMA hydrogel (left). *In vitro* fluorescent and NIR images of GelMA hydrogel degradation for 7 days with FITC and $NaYF_4$:Yb,Er@PAA UCNPs, respectively (right). (B) Plots of fluorescence intensity indicated by the gray value of each fluorescent image as showed in (A), calculated using Image J and the dry weight changes of hydrogels for 7 days. (C) Curve fitting between dry weight of hydrogels and PL intensity from UCNPs and FITC, respectively.

the strong tissue penetration capability of NIR light (up to 3.2 cm) that is not significantly absorbed by biological tissues [28]. Overall, the low cytotoxicity, high photostability and deep tissue penetration are of high importance to ensure the accuracy and reliability of $NaYF_4$:Yb,Er@PAA UCNPs in long-term *in vivo* hydrogel tracking.

3.3. In vitro tracking of GelMA degradation using UCNPs

One concern of using UCNPs as hydrogel tracker is the leakage of these physically mixed UCNPs, which may give unreliable predications in hydrogel degradation. To evaluate the feasibility and accuracy of $NaYF_4$:Yb,Er@PAA UCNPs in tracking hydrogels, the potential leakage of these UCNPs from GelMA hydrogels was studied by comparing the fluorescence intensity change between the UCNPs and FITC that was covalently modified on GelMA hydrogels (Fig. 3A). The tendency in the fluorescence intensity change of UCNPs matched with FITC during hydrogel degradation for 7 days, suggesting the reliability of UCNPs in labeling hydrogels without obvious leakage. Meanwhile, the dry weight of GelMA hydrogels in a parallel control group was measured as the standard degradation data and the change tendency of fluorescence intensity was in well agreement with the change tendency of dry weight of UCNP-FITC GelMA hydrogels (Fig. 3B), indicating the accuracy of UCNPs in long-term tracking of hydrogel degradation. We then further quantified the relationship between fluorescence intensity change and dry weight change through curve fitting and revealed a good linear

relationship (Fig. 3C), suggesting that the degradation of hydrogels was proportional to the fluorescence intensity decrease of UCNPs encapsulated in hydrogels. The degradation rate of GelMA hydrogel depends on both crosslinking density and enzymolysis environment. To evaluate the capability of UCNPs in tracking hydrogels with different degradation rates, GelMA hydrogels with different crosslink degrees were located in both hydrolysis and enzymolysis environment (Fig. S2A). The degradation rate was faster for hydrogel in enzymolysis environment as compared to that in only hydrolysis environment. Hydrogels with lower crosslink density processed faster degradation rate. This result indicates that the fast degradation was due to the easy infiltration of enzymes into the hydrogels with low crosslinking density while hydrogels with high crosslinking density limited enzyme diffusion, protecting the inner part of the hydrogel from degradation. These results are also in accordance with previous results reported in literature [21]. In addition, we measured the hydrogels dry weight and fluorescence intensity presented in a normalized linear graph (Fig. S2B-C). The accordant linear tendency of each group further proved the capability of UCNPs in accurate tracking of hydrogel degradation.

3.4. In vivo tracking of GelMA degradation using UCNPs

To evaluate the capability of UCNPs in tracking the hydrogel degradation *in vivo* in a real-time and non-invasive manner, we embedded the UCNPs and FITC dual labeled UCNP-FITC-GelMA hydrogels into rat abdomen and monitored the fluorescence intensity changes by fluorescence imaging for 7 days (Fig. 4A). Comparing NIR and UV channels, the fluorescence intensity of FITC was barely seen (Fig. 4B), mainly due to the limited tissue penetration of UV light. This observation is consistent with the tissue penetration result (Fig. 3). In contrast, the fluorescence intensity changes from UCNPs were clearly seen (Fig. 4B). The NIR excitation light (980 nm) and the red upconversion emission (655 nm) of $NaYF_4$:Yb,Er@PAA UCNPs both process deep tissue penetration ability, therefore the *in vivo* hydrogel degradation process can be easily tracked. In addition, information such as the size and location of implanted GelMA hydrogels can also be obtained. To evaluate the accuracy of $NaYF_4$:Yb,Er@PAA UCNPs in tracking the *in vivo* hydrogel degradation, the fluorescence intensity change of UCNPs was compared with the hydrogel dry weight change determined by the classic gravimetric method. Following the degradation of hydrogel, the fluorescence intensity of UCNPs decreased gradually and the tendency was matched with the decrease of hydrogel dry weight. The result confirmed that the fluorescence intensity change of UCNPs encapsulated within hydrogel indeed reflects the *in vivo* degradation of the embedded hydrogels. To further confirm the accuracy of UCNPs in *in vivo* hydrogel tracking, confocal images of tissue section slides from the implanted site were obtained and the fluorescence intensity changes from both

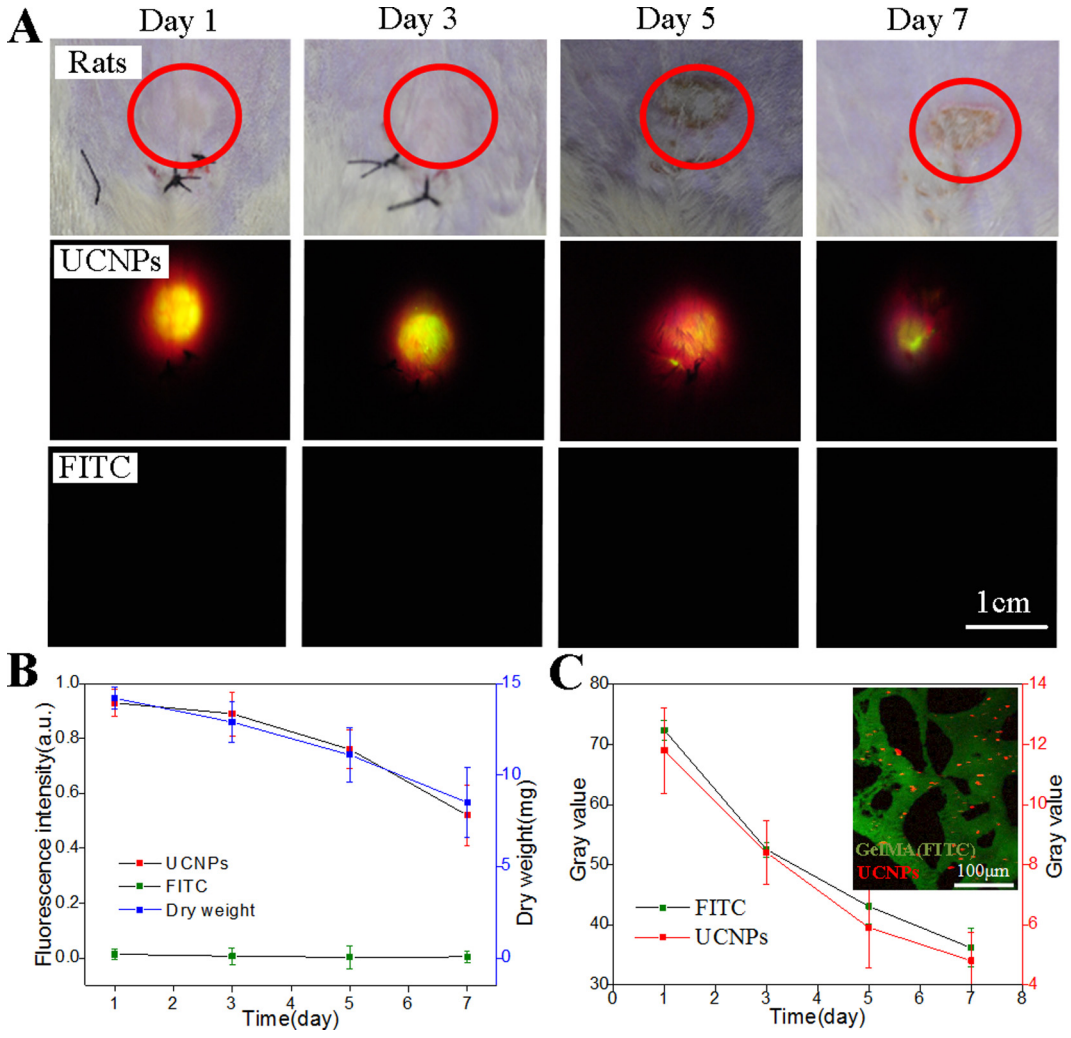

Fig. 4. *In vivo* tracking of the degradation of hydrogels using $NaYF_4$:Yb,Er@PAA UCNPs. (A) *In vivo* NIR image of UCNP and FITC dual labeled hydrogels transplanted into rat abdomens. (B) The relative PL intensity change of the NIR images as showed in (A) as compared to the dry weight change of the embedded hydrogels. (C) Plots of PL intensity calculated form confocal images taken from the tissue sections at the implanted sites. The insert shows confocal image of co-localization of UCNPs and FITC.

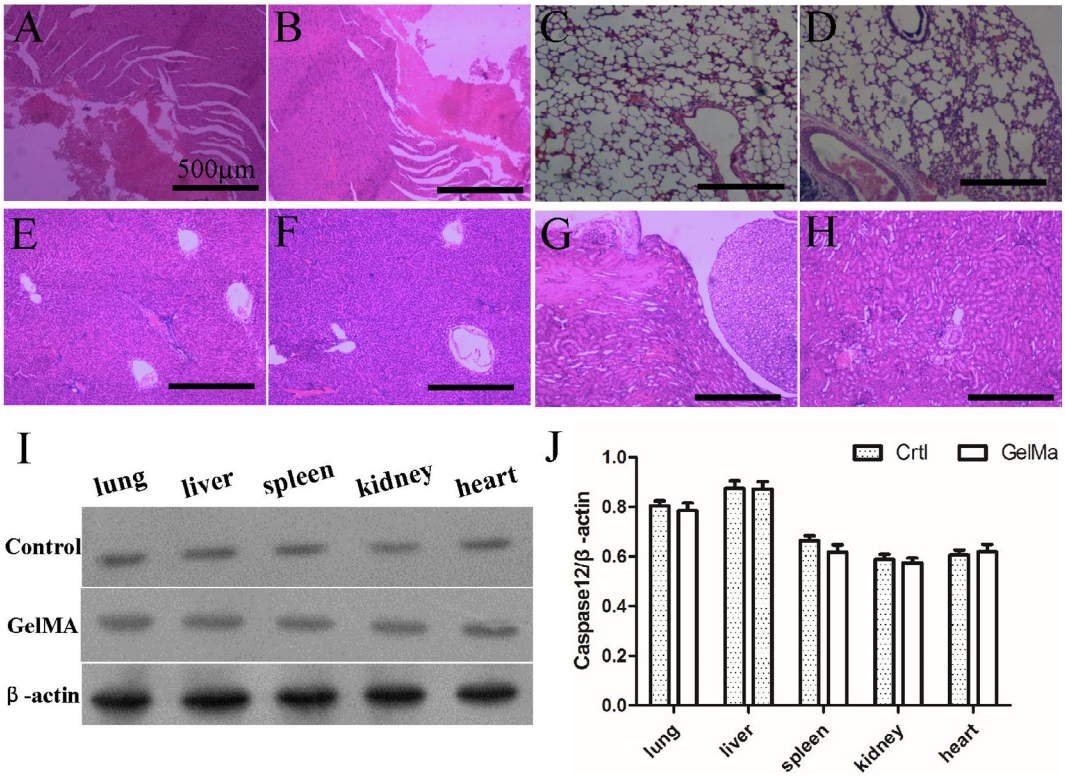

Fig. 5. *In vivo* safety study of UCNPs. The H&E staining of heart (A), lung (C), liver (E) and kidney (G) tissues from rats implanted with UNCP-labeled GelMA hydrogel implantation for 7 days, and heart (B), lung, (D) liver (F) and kidney (H) tissues obtained from rats without hydrogel implantation, respectively. (I) Western blot analysis of active cleaved caspase 12 in lung, liver, spleen, kidney and heart tissues obtained from rats with UNCP-labeled GelMA hydrogel implantation as compared to the control group without implantation. (J) WB bands were normalized to β-actin.

UCNPs and FITC were calculated. Both fluorescence intensity changes followed the same tendency, demonstrating the precise *in vivo* hydrogel tracking by UCNPs (Fig. 4C). Meanwhile, the UCNPs were found to situate uniformly within hydrogel network without leakage into the hydrogel pores (insert, Fig. 4C). To monitor the entire degradation cycle of UCNPs-encapsulated hydrogel, the *in vivo* hydrogel tracking was prolonged for 15 days. The fluorescent images of hydrogels that were embedded into rat abdomen were captured on day 3, 5, 10 and 15. On day 15, the fluorescence intensity of hydrogel in rat abdomen could hardly be detected. After dissection at the embedding site, the remained hydrogel was hard to distinguish and almost completely degraded (Fig. S3A-B). The results confirmed that UCNPs were able to accurately monitor the whole degradation process of the *in vivo* embedded hydrogels. With the help of UCNPs, precise *in vivo* monitoring of hydrogel degradation can be achieved, which provides a powerful tool in predicating the performance of hydrogels applied in drug delivery and tissue regeneration. It is good to know that cells from the host tissue were successfully infiltrated into GelMA hydrogels, demonstrating the good integration of GelMA with host tissue (Fig. S4A-B).

To further evaluate the *in vivo* safety of UCNPs as hydrogel tracking probes, we performed H&E staining to study the histopathological changes of the major organs (heart, lung, liver and kidney) and western blot analysis to study the caspase 12 expression (an inflammatory indicator) in various organs (lung, liver, spleen, kidney and heart tissues) from rats implanted with UCNP labeled hydrogels, using hydrogel-untreated rats as the control group. H&E staining results demonstrated that the key organs from both hydrogel-treated and untreated groups have integrated tissue structure without inflammation, edema and abnormal defects (Fig. 5). No significant histological differences were observed for the key organs obtained from both groups, suggesting the *in vivo* safety of employing UCNPs as fluorescent reporter for *in vivo* tracking hydrogel degradation. Additionally, we observed no significant difference in the expression of caspase 12 in the organs from hydrogel treated and untreated groups (Fig. 5I and J), suggesting the safety of using UCNPs as hydrogel tracking probes without causing obvious side effects.

4. Conclusion

To the best of our knowledge, this is the first contribution on real-time and non-invasive tracking of hydrogel degradation using upconversion emission signals from UCNPs both *in vitro* and *in vivo*. The feasibility of UCNPs for longitudinal and consecutive tracking of hydrogel degradation is evaluated against dry weight changes of hydrogels during degradation and further confirmed with the consistent fluorescent intensity changes from FITC that is covalently bonded to the polymer chain of hydrogels. As compared with FITC, UCNPs are more capable in realizing real-time tracking of hydrogel degradation due to the high tissue penetration capability of the excitation light over a 7-day period. The fluorescence changes of UCNPs and FITC from tissue slices are in the similar tendency, further confirming the accuracy of UCNPs in realizing longitudinal and consecutive tracking the *in vivo* degradation of hydrogels without causing any side effects. This study reported a facile and reliable way in reporting the *in vivo* distribution and degradation of hydrogels using UNCPs, which provides new opportunities for developing advanced NIR light regulated probes for clinical applications.

Conflicts of interest

The authors confirm that there is no conflict of interest.

Acknowledgements

This work was financially supported by the National Natural Science Foundation of China (11372243, 11522219, 11532009, 31600804), the China Postdoctoral Science Foundation (2016M592799) and the Fundamental Research Funds for the Central Universities (xjj2016081).

Appendix A. Supplementary data

Supplementary data associated with this article can be found, in the online version, at http://dx.doi.org/10.1016/j.actbio.2017.04.016.

References

[1] D.R. Griffin, W.M. Weaver, P.O. Scumpia, D.D. Carlo, T. Segura, Accelerated wound healing by injectable microporous gel scaffolds assembled from annealed building blocks, Nat. Mater. 14 (2015) 737–744.
[2] J.A. Burdick, W.L. Murphy, Moving from static to dynamic complexity in hydrogel design, Nat. Commun. 3 (2012) 1269.
[3] A. Paul, V. Manoharan, D. Krafft, A. Assmann, J.A. Uquillas, S.R. Shin, A. Hasan, M.A. Hussain, A. Memic, A.K. Gaharwar, A. Khademhosseini, Nanoengineered biomimetic hydrogels for guiding human stem cell osteogenesis in three dimensional microenvironments, J. Mater. Chem. B 4 (2016) 3544–3554.
[4] N. Huebsch, E. Lippens, K. Lee, M. Mehta, S.T. Koshy, M.C. Darnell, R. Desai, C.M. Madl, M. Xu, X. Zhao, O. Chaudhuri, C. Verbeke, W.S. Kim, K. Alim, A. Mammoto, D.E. Ingber, G.N. Duda, D.J. Mooney, Matrix elasticity of void-forming hydrogels controls transplanted-stem-cell-mediated bone formation, Nat. Mater. 14 (2015) 1269–1277.
[5] Y. Zhu, H. Jiang, S.H. Ye, T. Yoshizumi, W.R. Wagner, Tailoring the degradation rates of thermally responsive hydrogels designed for soft tissue injection by varying the autocatalytic potential, Biomaterials 53 (2015) 484–493.
[6] D. Druecke, E.N. Lamme, S. Hermann, J. Pieper, P.S. May, H.U. Steinau, L. Steninstraesser, Modulation of scar tissue formation using different dermal regeneration templates in the treatment of experimental full-thickness wounds, Wound Repair Regen. 12 (2004) 518–527.
[7] J.A. Reig, M.T.F. Figueras, L. Puig, Late-onset inflammatory adverse reactions related to soft tissue filler injections, Clin. Rev. Allergy Immun. 45 (2013) 97–108.
[8] N.Y. Tanyeri, M.H. Rich, M. Lee, M.H. Lai, J.H. Jeong, R.J. DeVolder, H. Kong, The spatiotemporal control of erosion and molecular release from micropatterned poly (ethylene glycol)-based hydrogel, Biomaterials 34 (2013) 8416–8423.
[9] J.P. Bruggeman, B.J. Bruin, C.J. Bettinger, R. Langer, Biodegradable poly (polyol sebacate) polymers, Biomaterials 29 (2008) 4726–4735.
[10] A.C. Grayson, G. Voskerician, A. Lynn, J.M. Anderson, M.J. Cima, R. Langer, Differential degradation rates in vivo and in vitro of biocompatible poly (lactic acid) and poly (glycolic acid) homo-and co-polymers for a polymeric drug-delivery microchip, J. Biomater. Sci.-Polym. E 15 (2004) 1281–1304.
[11] L.S.K. Sulzer, E.A. Waters, E.K. Kohlmeir, H. Kissler, X. Zhang, D.B. Kaufman, A.E. Barron, T.J. Meade, Protein polymer MRI contrast agents: longitudinal analysis of biomaterials in vivo, Magn. Reson. Med. 65 (2011) 220–228.
[12] A. Ahmadi, S.L. Thorn, E.I. Alarcon, M. Kordos, D.T. Padavan, T. Hadizad, G.O. Cron, R.S. Beanlands, J.N. DaSilva, M. Ruel, R.A. deKemp, E.J. Suuronen, PET imaging of a collagen matrix reveals its effective injection and targeted retention in a mouse model of myocardial infarction, Biomaterials 49 (2015) 18–26.
[13] A. Wickham, D. Sjölander, G. Bergström, E. Wang, V. Rajendran, C. Hildesjö, K. Skoglund, P. Nilsson, D. Aili, Near-infrared emitting and pro-angiogenic electrospun conjugated polymer scaffold for optical biomaterial tracking, Adv. Funct. Mater. 25 (2015) 4274–4281.
[14] M.L. James, S.S. Gambhir, A molecular imaging primer: modalities, imaging agents, and applications, Physiol. Rev. 92 (2012) 897–965.
[15] J.V. Jokerst, S.S. Gambhir, Molecular imaging with theranostic nanoparticles, Acc. Chem. Res. 44 (2011) 1050–1060.
[16] X. Ji, F. Peng, Y. Zhong, Y. Su, X. Jiang, C. Song, L. Yang, B. Chu, S.T. Lee, Y. He, Highly fluorescent, photostable, and ultrasmall silicon drug nanocarriers for long-term tumor cell tracking and in-vivo cancer therapy, Adv. Mater. 27 (2015) 1029–1034.
[17] G. Jin, D. Mao, P. Cai, R. Liu, N. Tomczak, J. Liu, X. Chen, D. Kong, D. Ding, B. Liu, K. Li, Conjugated polymer nanodots as ultrastable long-term trackers to understand mesenchymal stem cell therapy in skin regeneration, Adv. Funct. Mater. 25 (2015) 4263–4273.
[18] Y. Zhang, J. Yang, Design strategies for fluorescent biodegradable polymeric biomaterials, J. Mater. Chem. B 1 (2013) 132–148.
[19] N. Artzi, N. Oliva, C. Puron, S. Shitreet, S. Artzi, A.B. Ramos, A. Groothuis, G. Sahagian, E.R. Edelman, In vivo and in vitro tracking of erosion in biodegradable materials using non-invasive fluorescence imaging, Nat. Mater. 10 (2011) 704–709.
[20] X. Dong, C. Wei, T. Liu, F. Lv, Z. Qian, Real-time fluorescence tracking of protoporphyrin incorporated thermosensitive hydrogel and its drug release in vivo, ACS Appl. Mater. Inter. 8 (2016) 5104–5113.
[21] Y. Zhang, F. Rossi, S. Papa, M.B. Violatto, P. Bigini, M. Sorbona, F. Redaelli, P. Veglianese, J. Hilborn, D.A. Ossipov, Non-invasive in vitro and in vivo monitoring of degradation of fluorescently labeled hyaluronan hydrogels for tissue engineering applications, Acta Biomater. 30 (2016) 188–198.
[22] Y. Liu, J. Yang, P. Zhang, C. Liu, W. Wang, W. Liu, ZnO quantum dots-embedded collagen/polyanion composite hydrogels with integrated functions of degradation tracking/inhibition and gene delivery, J. Mater. Chem. 22 (2012) 512–519.
[23] Z. Zheng, M. Liu, S. Guo, J. Wu, D. Lu, G. Li, S.S. Liu, X.Q. Wang, D.L. Kaplan, Incorporation of quantum dots into silk biomaterials for fluorescence imaging, J. Mater. Chem. B 3 (2015) 6509–6519.
[24] D. Wang, J. Qian, S. He, J.S. Park, K.S. Lee, S. Han, Y. Mu, Aggregation-enhanced fluorescence in PEGylated phospholipid nanomicelles for in vivo imaging, Biomaterials 32 (2011) 5880–5888.
[25] K.T. Yong, W.C. Law, R. Hu, L. Ye, L. Liu, M.T. Swihart, P.N. Prasad, Nanotoxicity assessment of quantum dots: from cellular to primate studies, Chem. Soc. Rev. 42 (2013) 1236–1250.
[26] W. Wang, J. Liu, C. Li, J. Zhang, J. Liu, A. Dong, D. Kong, Real-time and non-invasive fluorescence tracking of in vivo degradation of the thermosensitive PEGylated polyester hydrogel, J. Mater. Chem. B 2 (2014) 4185–4192.
[27] K. Szacilowski, W. Macyk, A.D. Matuszek, M. Brindell, G. Stochel, Bioinorganic photochemistry: frontiers and mechanisms, Chem. Rev. 105 (2005) 2647–2694.
[28] G. Chen, J. Shen, T.Y. Ohulchanskyy, N.J. Patel, A. Kutikov, Z. Li, J. Song, R.K. Pandey, H. Ågren, P.N. Prasad, G. Han, (α-NaYbF4: Tm3+)/CaF2 core/shell nanoparticles with efficient near-infrared to near-infrared upconversion for high-contrast deep tissue bioimaging, ACS Nano 6 (2012) 8280–8287.
[29] Y.F. Wang, G.Y. Liu, L.D. Sun, J.W. Xiao, J.C. Zhou, C.H. Yan, Nd3+-sensitized upconversion nanophosphors: efficient in vivo bioimaging probes with minimized heating effect, ACS Nano 7 (2013) 7200–7206.
[30] S. Zeng, M.K. Tsang, C.F. Chan, K.L. Wong, J. Hao, PEG modified BaGdF 5: Yb/Er nanoprobes for multi-modal upconversion fluorescent, in vivo X-ray computed tomography and biomagnetic imaging, Biomaterials 33 (2012) 9232–9238.
[31] X. Xie, N. Gao, R. Deng, Q. Sun, Q.H. Xu, X. Liu, Mechanistic investigation of photon upconversion in Nd3+-sensitized core–shell nanoparticles, J. Am. Chem. Soc. 135 (2013) 12608–12611.
[32] Y. Ma, Y. Ji, M. You, S. Wang, Y. Dong, G. Jin, M. Lin, Q. Wang, A. Li, X. Zhang, F. Xu, Labeling and long-term tracking of bone marrow mesenchymal stem cells in vitro using NaYF4: Yb 3+, Er 3+ upconversion nanoparticles, Acta Biomater. 42 (2016) 199–208.
[33] N.M. Idris, Z. Li, L. Ye, E.K.W. Sim, M. Rahendran, P.C.L. Ho, Y. Zhang, Tracking transplanted cells in live animal using upconversion fluorescent nanoparticles, Biomaterials 30 (2009) 5104–5113.
[34] G. Jalani, R. Naccache, D.H. Rosenzweig, S. Lerouge, L. Haglund, F. Vetrone, M. Cerruti, Real-time, non-invasive monitoring of hydrogel degradation using LiYF 4: Yb 3+/Tm 3+ NIR-to-NIR upconverting nanoparticles, Nanoscale 7 (2015) 11255–11262.
[35] J. Sun, D.H. Kim, Y. Guo, Z. Teng, Y. Li, L. Zheng, Z. Zhang, A.C. Larson, G. Lu, A c (RGDfE) conjugated multi-functional nanomedicine delivery system for targeted pancreatic cancer therapy, J. Mater. Chem. B 3 (2015) 1049–1058.
[36] J. Wu, X. Zhao, D. Wu, C.C. Chu, Development of a biocompatible and biodegradable hybrid hydrogel platform for sustained release of ionic drugs, J. Mater. Chem. B 2 (2014) 6660–6668.
[37] H. Chen, L. Guo, J. Wicks, C. Ling, X. Zhao, Y. Yan, J. Qi, W. Cui, L. Deng, Quickly promoting angiogenesis by using a DFO-loaded photo-crosslinked gelatin hydrogel for diabetic skin regeneration, J. Mater. Chem. B 4 (2016) 3770–3781.
[38] X. Zhao, Q. Lang, L. Yildirimer, Z.Y. Lin, W. Cui, N. Annabi, K.W. Ng, M.R. Dokmeci, A.M. Ghaemmaghami, A. Khademhosseini, Photocrosslinkable gelatin hydrogel for epidermal tissue engineering, Adv. Healthcare Mater. 5 (2016) 108–118.
[39] X. Zhao, S. Liu, L. Yildirimer, H. Zhao, R. Ding, H. Wang, W. Cui, D. Weitz, Injectable stem cell-laden photocrosslinkable microspheres fabricated using microfluidics for rapid generation of osteogenic tissue constructs, Adv. Funct. Mater. 26 (2016) 2809–2819.
[40] S.J. Bradd, M.J. Dunn, Analysis of membrane proteins by Western blotting and enhanced chemiluminescence, Methods Mol. Biol. 19 (1993) 211–218.
[41] P. Ziółkowski, E. Gamian, B. Osiecka, A. Zougman, J.R. Wiśniewski, Immunohistochemical and proteomic evaluation of nuclear ubiquitous casein and cyclin-dependent kinases substrate in invasive ductal carcinoma of the breast, Biomed. Res. Int. 3 (2009) 919645.
[42] X. Ye, J.E. Collins, Y. Kang, J. Chen, D.T. Chen, A.G. Yodh, C.B. Murray, Morphologically controlled synthesis of colloidal upconversion nanophosphors and their shape-directed self-assembly, Proc. Natl. Acad. Sci. U.S.A. 107 (2010) 22430–22435.
[43] M. Wang, C.C. Mi, J.L. Liu, X.L. Wu, Y.X. Zhang, W. Hou, F. Li, S.K. Xu, One-step synthesis and characterization of water-soluble NaYF4:Yb, Er/Polymer nanoparticles with efficient up-conversion fluorescence, J. Alloy. Compd. 485 (2009) L24–L27.
[44] H. Hu, L. Xiong, J. Zhou, F. Li, T. Cao, C. Huang, Multimodal-luminescence core-shell nanocomposites for targeted imaging of tumor cells, Chem. Eur. J. 15 (2009) 3577–3584.

[45] M. Hu, J. Zhao, X. Ai, M. Budanovic, J. Mu, R.D. Webster, Q. Cao, Z. Mao, B. Xing, Near infrared light-mediated photoactivation of cytotoxic Re (I) complexes by using lanthanide-doped upconversion nanoparticles, Dalton Trans. 45 (2016) 14101–14108.
[46] Y. Gu, X. Qiao, J. Zhang, Y. Sun, Y. Tao, S. Qiao, Effects of surface modification of upconversion nanoparticles on cellular uptake and cytotoxicity, Chem. Res. Chin. Univ. 32 (2016) 474–479.
[47] Y. Su, M. Hu, C. Fan, Y. He, Q. Li, W. Li, L. Wang, P. Shen, Q. Huang, The cytotoxicity of CdTe quantum dots and the relative contributions from released cadmium ions and nanoparticle properties, Biomaterials 31 (2010) 4829–4834.
[48] A.I.V.D. Bulcke, B. Bogdanov, N.D. Rooze, E.H. Schacht, M. Cornelissen, H. Berghmans, Structural and rheological properties of methacrylamide modified gelatin hydrogels, Biomacromolecules 1 (2000) 31–38.